Performance analysis of GMSK Carrier synchronization loop phase detector at very low SNR

Mohamed Amine Jhaidri, Alain Thomas, Christophe Laot

PERFORMANCE ANALYSIS OF GMSK CARRIER SYNCHRONIZATION LOOP PHASE DETECTOR AT VERY LOW SNR

Mohamed Amine Jhaidri[(1), (2)], **Alain Thomas**[(1)], **Christophe Laot**[(2)]

[(1)]***Zodiac Data Systems***
5 Avenue des Andes, 91940 Les Ulis, France
Email: firstname.lastname@zodiacaerospace.com

[(2)]***Institut Mines-Telecom; Telecom Bretagne; UMR CNRS 6285 Lab-STICC***
Technopôle Brest Iroise 29238 Brest Cedex, France
Email: firstname.lastname@telecom-bretagne.eu

I. INTRODUCTION

Deep space communication systems operate on very long distance and the on-board energy generator capacity is very limited which results a very low signal to noise ratio (SNR) at the reception. This is the reason why near Shannon limit error correcting codes are used. Nevertheless, to take advantage of this gain, the coherent demodulation is mandatory and the carrier phase synchronization must be provided at a more restrictive SNR ($E_s/N_0 \simeq -8$ dB for a Turbo-code 1/6).
Spectrum resources allocated for deep space missions are limited (X-band at 8 GHz), and in order to optimize the spectral efficiency, the Consultative Committee for Space Data System (CCSDS) recommended [1] pre-coded GMSK modulation (Gaussian Minimum Shift Keying) with Gaussian filter bandwidth-bit period product $BT_b = 0.5$ for Category B missions (deep space missions) and GMSK $BT_b = 0.25$ for category A missions (low altitude missions).
This paper discusses a blind phase detector [2] derived from maximum *a posteriori* (MAP) criterion and Laurent expansion [3] for GMSK modulation. In order to evaluate the performance of this phase detector in a closed loop structure at very low SNR, we consider two others simplified versions that have been described in [4] and [5]. We develop a comprehensive study of these three different structures in both linear and nonlinear domains. We also present the results obtained by computer simulation using low rate error-correction code (Turbo 1/6). The aim of this work is to compare the performance of these three phase detectors and estimate the impact of the simplification that have been made to obtain the two simplified versions.

II. SYSTEM DESCRIPTION

Fig.1, illustrates a block diagram of the precoded GMSK communication system. The system consists of a binary data source (delivering the information bits d_k), a data precoder, a GMSK modulator and a coherent receiver with carrier phase recovery schemes. The clock offset is assumed to be perfectly estimated and equal to zero.
GMSK is a continuous phase modulation (CPM) having several interesting properties such as constant envelope which allows the amplifier to operate in full-saturation mode and maximizes the conversion efficiency without undergoing any form of spectral distortion. The pre-coding is used to eliminate the inherent differential decoding and therefore improve the bit error rate (BER) of the demodulator.

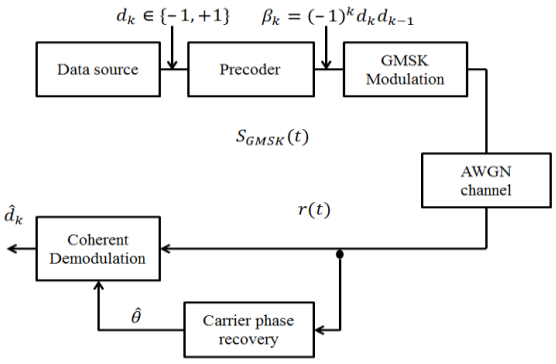

Fig. 1. GMSK communication system

Using Laurent expansion, the complex base-band envelope of the GMSK $BT_b = 0.5$ signal can be represented by a superposition of two amplitude-modulation pulses (AMP).

$$S_{GMSK}(t) = \sqrt{\frac{E_b}{T_b}} \sum_{k=0}^{N-1} \{a_{0,k} C_0(t - kT_b) + a_{1,k} C_1(t - kT_b)\} \tag{1}$$

where E_b is the average energy per bit, $1/T_b$ is the bit rate, $\{a_{0,k}, a_{1,k}\}$ are the data symbols and $\{C_0, C_1\}$ are Laurent pulses. The duration of the main pulse $C_0(t)$ is $3T_b$ while the second pulse $C_1(t)$ has a duration of T_b.

$$a_{0,k} = \prod_{n=0}^{k} j\beta_n = j\beta_k a_{0,k-1} \tag{2}$$

$$a_{1,k} = j\beta_k a_{0,k-2} \tag{3}$$

with $\beta_k = (-1)^k d_k d_{k-1}$, obtained by a differential encoding of the information date bits d_k as presented in Fig.1.

III. CARRIER PHASE SYNCHRONIZATION LOOP

The received signal $r(t)$ is defined as follows:

$$r(t) = S_{GMSK}(t) e^{j\theta(t)} + n(t) \tag{4}$$

where $n(t)$ is an additive white Gaussian noise (AWGN) with single-side PSD N_0 W/Hz. The phase difference $\phi(t)$ between the carrier phase $\theta(t)$ and the phase of the receiver oscillator $\hat{\theta}(t)$ degrades the system BER performance. Therefore, to satisfy the required transmission quality, we need to estimate the carrier phase and use it to optimally demodulate the received signal. According to maximum *a posteriori* (MAP) estimation criterion, the most likely phase $\hat{\theta}$ is that which maximizes the *a posteriori* probability $p(\hat{\theta}(t)|r(t))$. The carrier phase $\theta(t)$ is assumed to be uniformly distributed over the interval $[-\pi, \pi]$, which means that maximizing $p(\hat{\theta}(t)|r(t))$ is equivalent to maximizing $p(r(t)|\hat{\theta}(t))$ (maximum-likelihood ML estimation). In the case of GMSK $BT_b = 0.5, 99.97\%$ of the signal energy is carried by the first Laurent pulse C_0. Therefore, in order to simplify the receiver complexity, we ignore the second pulse C_1. For an AWGN channel the likelihood probability has the form:

$$p\big(r(t)\big|\hat{\theta}(t)\big) \propto exp\left(-\frac{1}{N_0}\int_0^{T_0} r(t) S^*_{GMSK}\big(t, \hat{\theta}(t), \hat{\boldsymbol{a}}\big) dt\right) \tag{5}$$

where $[0, T_0]$ is the observation interval and $\{\hat{\boldsymbol{a}}, \hat{\theta}(t)\}$ are the estimates of the parameters that need to be determined. To arrive at the blind closed loop carrier phase synchronizer, we consider a sliding window implementation of the MAP carrier phase estimator. In other words, we decompose the observation period $[0, T_0]$ into a set of sub-periods with time length equal to $K_b T_b$. During the k^{th} sub-observation periods $[kT_b, (k + K_b)T_b]$ we assume that the carrier phase $\theta(t)$ is constant and equal to θ_k. Afterward, at each instant kT_b we take the natural logarithm of the likelihood probability (5) calculated over the time interval $kT_b \le t \le (k + K_b)T_b$ and averaged over the data sequence $\hat{\boldsymbol{a}}$, differentiate it with respect to the estimated phase at this interval $\hat{\theta}_k$ and finally use this as an estimation error signal $e_{BMAP}(\phi_k)$, where $\phi_k = \theta_k - \hat{\theta}_k$: is the phase offset. By tacking $K_b = 4$ and considering only the even instants (k is even), we obtain:

$$e_{BMAP}(\phi_k) = -\sum_{\substack{l=k-2 \\ l:even}}^{k+2} \Re\big(I_{l,k}\big) \tanh\big(\Im\big(I_{l,k}\big)\big) + \sum_{\substack{l=k-1 \\ l:odd}}^{k+3} \Im\big(I_{l,k}\big) \tanh\big(\Re\big(I_{l,k}\big)\big) \tag{6}$$

$$I_{l,k} = \frac{2}{N_0}\sqrt{E_b/T_b} \quad \left\{\int_{kT_b}^{(k+4)T_b} r(t) C_0(t - lT_b) \; dt\right\} e^{-j\hat{\theta}_k} \tag{7}$$

Fig. 2 shows a block diagram for the GMSK blind carrier phase synchronization loop. The system consists of phase detector defined by (6), a proportional-integrator loop filter (LF) whose transfer function is described by (8) and a numerically controlled oscillator (NCO).

$$F(s) = K_f\left(1 + \frac{\alpha}{s}\right) \tag{8}$$

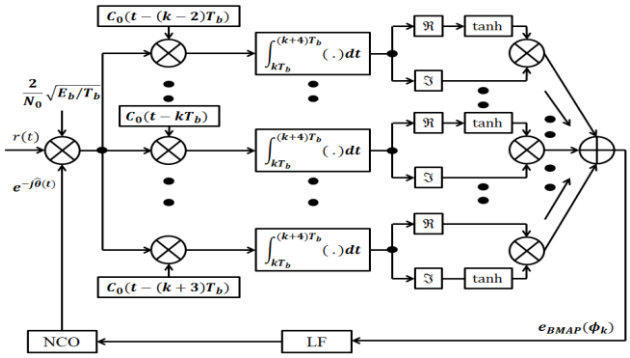

Fig. 2. GMSK blind carrier phase synchronization loop

where K_f is the loop filter gain and α is the loop filter integrator constant. These parameters will be set according to the mission constraints (Doppler, Doppler rate, phase error variance, acquisition time).
From the blind MAP (BMAP) detector, the assumptions that lead to the two suboptimal versions of the carrier phase loop are as follows:

1) The most part of the phase error (6) energy is concentrated in the terms corresponding to $l = k$ and $l = k + 1$, the contribution of the other terms is negligible.

$$e_{BMAP}(\phi_k) \simeq -\Re(I_{k,k})\tanh\left(\Im(I_{k,k})\right) + \Im(I_{k+1,k})\tanh(\Re(I_{k+1,k})) \tag{9}$$

2) At very low SNR, the nonlinear hyperbolic tangent function can be approximated by a linear function as $\tanh(x) \simeq x$.

$$e_{SDD}(\phi_k) = -\Re(I'_{k,k})\Im(I'_{k,k}) + \Re(I'_{k+1,k})\Im(I'_{k+1,k}) \tag{10}$$

3) At high SNR, hyperbolic tangent function can be approximated by the "sign" function as $\tanh(x) \simeq sign(x)$.

$$e_{HDD}(\phi_k) = -\Re(I'_{k,k})sign\left(\Im(I'_{k,k})\right) + \Im(I'_{k+1,k})sign(\Re(\Im(I'_{k+1,k})) \tag{11}$$

Once the hyperbolic tangent function is approximated either by the linear function or the function "*sign*", the division of the I_k's by $N_0/2$, which was used to place the I_k's in the appropriate region of the "*tanh"* function (linear or constant region) based on SNR, becomes useless. Therefore, we introduce the new variables $I_k{}' = I_k N_0/2$ and $I'_{k+1} = I_{k+1}N_0/2$ which do not depend on SNR. Fig. 3, shows the block diagrams of the two simplified GMSK carrier phase synchronization loop based on the low (Fig. 3 (a)) and the high (Fig. 3 (b)) SNR approximation of the nonlinear hyperbolic tangent function. The phase detector based on the high SNR approximation is a hard-decision directed (HDD) detector while the second one is a soft-decision directed (SDD) detector. After having presented the different GMSK phase detectors, we detail in the next part of this papier a comprehensive study covering both linear and nonlinear operating domain. Firstly, we need to characterize the phase detectors by the so-called S-curve in order to define the equivalent models of these carrier phase loops and correctly set their parameters (equivalent noise bandwidth, damping factor…).

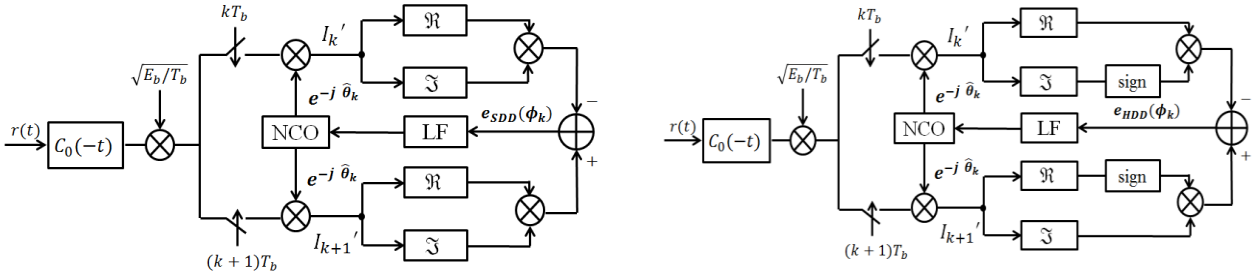

(a) Low SNR *tanh* approximation based carrier loop (b) High SNR *tanh* approximation based carrier loop

Fig. 3. Sup-optimal versions of the GMSK blind MAP carrier phase synchronizer

IV. S-CURVES DETERMINATION

By definition the S-curve $S(\phi)$ is the average value of the phase detector output in the presence of a constant offset between the carrier phase and the phase generated by the receiver N.C.O in an open loop structure:

$$S(\phi) = E[e(\phi)|\phi] \tag{12}$$

The S-curve expressions of the two sup-optimal GMSK $BT_b = 0.5$ carrier phase loop using the definition (12) are given below. These expression present a contribution of this work since, to the best of our knowledge, they do not exist in the literature. For the lack of space, we will not detail the calculation.

$$S_{SDD}(\phi) = E[e_{SDD}(\phi)|\phi] = E_b^2(R(0)^2 - 2R(1)^2)\sin(2\phi) \tag{13}$$

$$R(m) = \frac{1}{T_b}\int_0^{3T_b} C_0(t)C_0(t - mT_b)dt \tag{14}$$

$$S_{HDD}(\phi) = E\left[e_{2,k}(\phi)\middle|\phi\right] = \frac{1}{2}U_1(2P_1 - 1) + U_2(2P_2 - 1) + \frac{1}{2}U_3(2P_3 - 1) \tag{15}$$

where

$$U_1 = -2R(1)\cos(\phi) + R(0)\sin(\phi)\,; P_1 = \frac{1}{2}erfc\left(-\sqrt{\frac{E_bR(0)}{2N_0}}(2R(1)\sin(\phi) + R(0)\cos(\phi))\right) \tag{16}$$

and

$$U_2 = R(0)\sin(\phi)\ ;\ P_2 = \frac{1}{2}erfc\left(-\sqrt{\frac{E_bR(0)}{2N_0}}(R(0)\cos(\phi))\right) \tag{17}$$

and

$$U_3 = 2R(1)\cos(\phi) + R(0)\sin(\phi)\,;\ P_1 = \frac{1}{2}erfc\left(-\sqrt{\frac{E_bR(0)}{2N_0}}(-2R(1)\sin(\phi) + R(0)\cos(\phi))\right) \tag{18}$$

Fig. 4. shows the S-curves of the three considered detectors for the GMSK $BT_b = 0.5$. Contrary to the BMAP and the HDD detector, the SDD detector S-curve does not depend on the SNR (as expected from the theory). In hardware implementation, this property is a very important advantage since we don't have to estimate the SNR in order to set the PLL parameters which depend on the S-curve expression. At very low SNR ($E_s/N_0 < 0$) , the three phase detector S-curves are proportional to $sin(2\phi)$ (semi-sinusoidal detector).

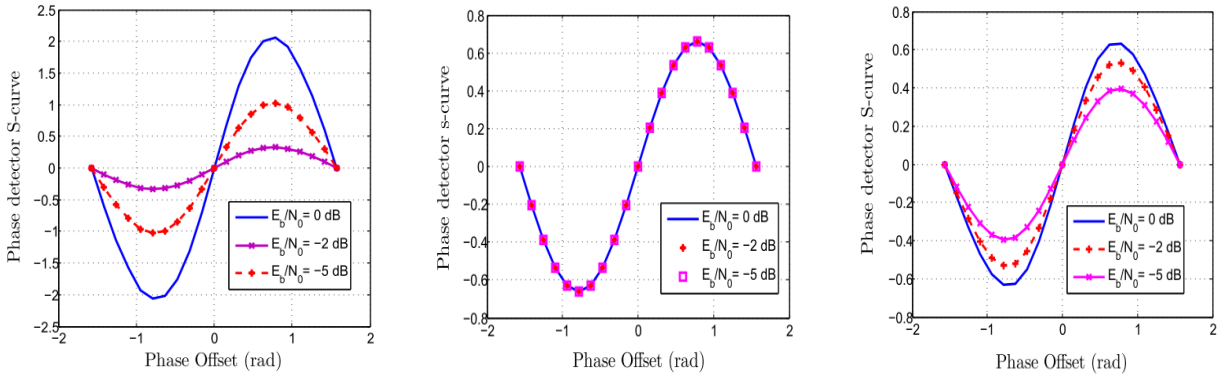

(a) BMAP phase detector S-curve (b) SDD phase detector S-curve (c) HDD phase detector S-curve

Fig. 4. Phase detectors S-curves

V. NONLINEAR ACQUISITION PHASE

In this section we present a new study of the nonlinear acquisition phase of a carrier phase loop having a semi-sinusoidal phase detector S-curve ($S(\phi) \propto sin(2\phi)$) which is the case of the three considered phase detectors S-curves at very low SNR. This study is based on the phase plan method [6] which is a graphical method for nonlinear system analysis. In the literature we find several analyses of sinusoidal carrier phase loop ($S(\phi) \propto sin(\phi)$) but these results are not directly applicable to our case.

A block diagram of the carrier phase loop nonlinear equivalent model is shown in Fig. 5, where θ and $\hat{\theta}$ are the instantaneous phases of the carrier signal and that of the N.C.O signal, respectively, $e(t)$ represents the error signal and $u(t)$ the loop filter output (or the N.C.O command signal). K_v is known as the N.C.O gain. Note that this analysis has been developed in the continuous time domain. However, the transformation (dividing the loop parameters by the sampling period) used for the digital transition does not directly influence the behavior of the system and the obtained results remain applicable.

Firstly we consider the case of a phase ramp input, i.e.

$$\theta(t) = \Delta\omega t + \theta_0 \tag{19}$$

where $\Delta\omega = \omega_i - \omega_0$ is frequency offset between the carrier signal and the N.C.O signal and θ_0 is the phase offset at $t = 0$. Using the model above, we can express the differential equation governing the system behaviour in the nonlinear phase as:

$$\frac{d^2\phi(t)}{d\tau^2} + 2\cos\big(2\phi(t)\big)\frac{d\phi(t)}{d\tau} + \alpha' \sin\big(2\phi(t)\big) = 0 \tag{20}$$

where α' is the loop filter integrator constant α normalized by the loop gain $G = K_d K_f K_v$ and $\tau = Gt$. The system equation (20) is a second-order nonlinear differential equation which does not have a known analytic solution. Therefore, the phase plan method is used to analyse the system nonlinear behaviour. Decomposing (20) in a set of equation as follows:

$$\begin{cases} \dfrac{d\phi(t)}{dt} = \dot{\phi}(t) & \text{(21.a)} \\ \dfrac{d\dot{\phi}(t)}{dt} = -2\cos\big(2\phi(t)\big)\dfrac{d\phi(t)}{dt} - \alpha' \sin\big(2\phi(t)\big) & \text{(21.b)} \end{cases}$$

where $\big(\phi(t), \dot{\phi}(t)\big)$ are the phase and the frequency error, respectively.

- **Equilibrium points :**

By definition, $M(\phi_0, \dot{\phi}_0)$ is an equilibrium point for the system described by (21) if it satisfies the following conditions:

$$\begin{cases} \dfrac{d\phi_0(t)}{dt} = 0 \\ \dfrac{d\dot{\phi}_0(t)}{dt} = 0 \end{cases} \tag{22}$$

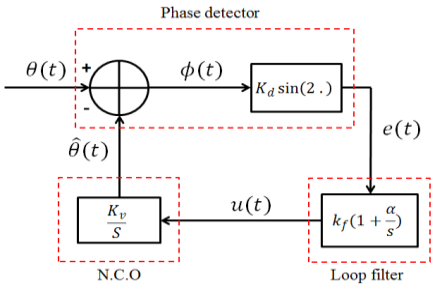

Fig. 5. Nonlinear carrier phase loop equivalent model

Then the equilibrium point is defined as follows:

$$\begin{cases} \phi_0 = \dfrac{n\pi}{2}, n \in 2\mathbb{Z} \\ \dot{\phi}_0 = 0 \end{cases} \tag{23}$$

According to (23), once the locked state is reached, the frequency offset ($\dot{\phi}$) will be completely eliminated but the loop could lock on the opposite phase since the points $M(\phi = m\pi, \dot{\phi} = 0), m = 1,3,5$ ..., are stable equilibrium points. Therefore, a phase ambiguity resolution technique must be used. By dividing (21.b) by (21.a) we obtain

$$\frac{d\dot{\phi}(t)}{d\phi(t)} = -2\cos(2\phi(t)) - \frac{\alpha' \sin(2\phi(t))}{\dot{\phi}(t)} \tag{24}$$

For an initial condition $M\left(\phi(t=0), \dot{\phi}(t=0)\right)$ the equation (24) allows us to calculate (by using a numerical calculator) the tangent at each instant t_0 and thus to obtain point by point the trajectory describing the evolution of the phase and the frequency offset during the time. By moving the initial point M_0 and using this approach, we can plot the so-called phase plane of the carrier phase loop. Fig.6 shows the phase plane of the carrier phase loop around the equilibrium point $M_0(\phi = 0, \dot{\phi} = 0)$, and during the first period ($\phi \in [-\pi/2, \pi/2]$) for $\alpha' = 1$ (this value corresponds to a damping equal to $1/\sqrt{2}$ usually used in practice [7]).

- **Lock-in range :**

Assuming that the PLL is initially in locked state (in an equilibrium point of the phase plane). The pull-out frequency Ω_{po} is defined as the maximum value (in absolute value) of the frequency offset that may arise between the NCO and the carrier signal and still the carrier loop is able to relock without slipping any cycle (return to the same equilibrium point). Exceeding this frequency, the PLL will slip one or more cycle (pull-in process) before reaching another stable equilibrium point (relocking). The frequency interval $[-\Omega_{po}, \Omega_{po}]$ is known as the lock-in range in the PLL theory. The pull-in process can be too slowly and unreliable for many applications.

Therefore, the lock-in range is a very important parameter to satisfy the required transmission constraints. Using the phase plane, the pull-out frequency can be determined as the intersection of the frequency axis and the separatrix trajectories (the trajectories plotted in red on Fig.6 dividing the phase plan around the equilibrium point into two parts, spiral trajectories and sinusoidal trajectories).

In order to simplify the loop parameters setting according to the desired performance, we have expressed the PLL pull-out frequency as a function of the normalized loop filter integrator constant as follows:

$$\Omega_{po} = 1.24G(0.74 + \sqrt{\alpha'}) \tag{25}$$

- **Pull-in Time :**

Starting from an initial frequency offset $\dot{\phi}_0$ larger than the pull-out frequency, the time required for the carrier phase loop to arrive at an equilibrium stable point (locked state) is known as the pull-in time.

By making the same assumptions [7] that have been used in the case of the sinusoidal PLL, we derived an approximate analytic expression of the pull-in time as follows:

$$T_{pull} = \frac{\dot{\phi}_0^2}{\alpha G^2} \tag{26}$$

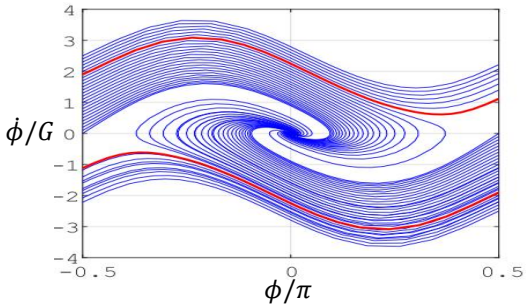

Fig. 6. Phase plan of a semi-sinusoidal PLL

Using (25) and (26) we are able to well configure the carrier phase loop parameters (closed-loop gain and filter loop integrator constant) and assure the system performance in terms of acquisition time.
In the presence of Doppler rate F_r, the system equilibrium stable points become:

$$\begin{cases} \phi_0 = \dfrac{n\pi}{2} + 0.5\sin^{-1}\left(\dfrac{2\pi F_r}{\alpha G}\right), n \in 2\mathbb{Z} \\ \dot{\phi}_0 = 0 \end{cases} \tag{27}$$

In the presence of Doppler rate effect, a second order PLL is not able to perfectly synchronize the receiver N.C.O with the carrier signal. Therefore, we have to use a third order PLL (with a second loop filter integrator) or a Doppler compensation technique to avoid the non-zero phase offset in tracking phase which degrades the system BER performance. In some missions, a threshold of BER degradation can be tolerated. In this case, (27) allows us to define a lower bound for G and α.

VI. LINEAR TRACKING PHASE

In tracking phase (near zero phase offset) the phase detector S-curve can be approximated by its slope at the origin $(dS/d\phi|\phi = 0)$ and the PLL equivalent model become a linear model. The transfer function of the system is defined as:

$$H(s) = \frac{2Gs + 2G\alpha}{s^2 + 2Gs + 2G\alpha} \tag{28}$$

Using (28) and the canonical second order system transfer function, we can express the loop parameters as:

$$\begin{cases} K_f = \xi\omega_n/K_d \\ \alpha = \omega_n/(2\xi) \end{cases} \tag{29}$$

where ω_n is the natural frequency and ζ is the damping factor. For a second order PLL, the one-side noise equivalent bandwidth B_L is defined by:

$$B_L = \frac{\omega_n}{2}\,\zeta\left(1 + \frac{1}{4\zeta^2}\right) \tag{30}$$

Using the PLL linear model parameters, the pull-in frequency can be rewritten:

$$\Omega_{po} \simeq 0.88\omega_n(\zeta + 1) \tag{31}$$

And the pull-in time:

$$T_{pull} \simeq \frac{2\dot{\phi}_0^2}{\zeta\omega_n^3} \tag{32}$$

From (31) and (32), we notice that a sinusoidal PLL has nearly two times larger lock-in range and four times faster pull-in process than a semi-sinusoidal PLL having the same noise equivalent bandwidth.

Once the tracking phase is reached, we can evaluate the receiver performance and compare the different phase detectors. Fig.7 (a) illustrates the phase error variance of the three phase detector in tracking phase for $B_L = 0.05\%B_r$ (B_r: Bit rate), this equivalent noise bandwidth is commonly used in practice [9]. For $E_s/N_0 < -5dB$, the BMAP and SDD phase detectors have nearly the same performance while $\sim$ 2dB degradation could be noticed between these detectors and the HDD detector. This degradation comes from the inappropriate approximation of the "$tanh$" by the function "$sign$" in this range of SNR. Otherwise, for higher SNR ($E_s/N_0 \geq -2\,dB$) this approximation gives a better performance than the linear one and the HDD variance curve approaches that of BMAP detector while the SDD phase error variance is degrading. Fig.7 (b) shows the system BER performance corresponding to each phase detector using a turbo code 1/6 and a frame length of 8920 bits. This FEC requires carrier phase synchronization at very low SNR ($E_s/N_0 \simeq -0.2 + 10\,log_{10}(1/6) \simeq -8dB$) to take advantage of its coding gain. The HDD detector error variance loss affects directly the BER with a degradation of 0.1 dB for a BER $= 10^{-5}$.

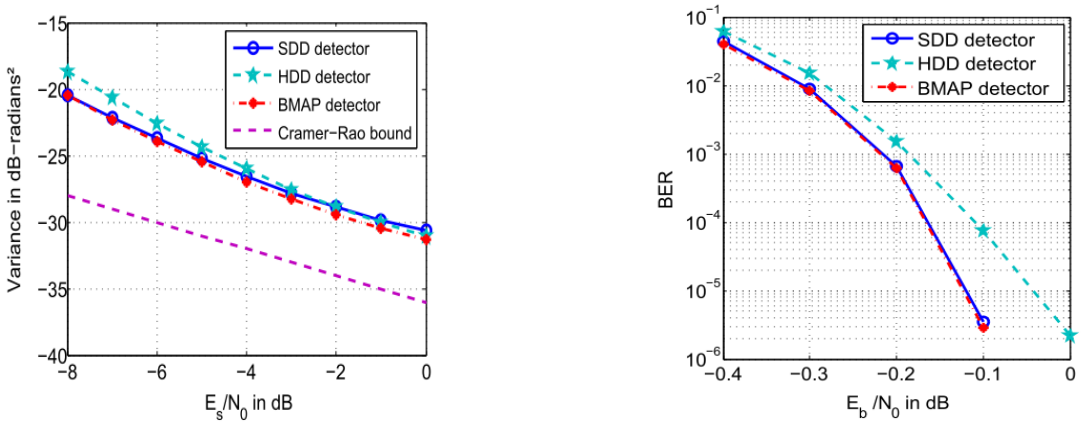

(a) Phase error variance in tracking phase (b) BER of a Turbo code (8920,1/6)

Fig. 7. GMSK $BT_b = 0.5$ carrier phase loops tracking performance

From a point of view of hardware integration, choosing the BMAP phase detector increases the implementation complexity. In fact, an automatic gain control (AGC) must be included at each multiplier (6 multipliers for GMSK $BT_b = 0.5$ against two AGC inside the carrier loop for the SDD and HDD detectors) output (see Fig.2) to compensate the power loss caused by the Analog-to-Digital converter when the noise power is important.
Furthermore, the iterative Cordic algorithm [8] must be used to calculate the nonlinear "$tanh$" function and the SNR has to be blindly estimated (same for the HDD detector) in order to correctly set the loop parameters as a function of the phase detector S-curve. Taking into account the implementation complexity and the obtained performance, The SDD detector represents the best candidate for the deep space mission characterized by a very low SNR and Non-data aided transmission.

VII. CONCLUSION

In this paper, a blind GMSK carrier phase loop based on the MAP estimation criterion has been presented as well as two others simplified versions. The analytic expressions of the S-curves have been derived and compared to computer simulations. Using this expressions and the phase plan method, a nonlinear analysis of a semi-sinusoidal carrier phase loop was developed and several results were obtained. In order to compare the different phase detectors in the tracking phase, an evaluation in terms of phase error variance and BER in turbo coded structure has been carried out and it has been shown that at very low SNR ($E_s/N_0 \simeq -8\,dB$) the SDD detector performance in tracking phase is indistinguishable from that of BMAP detector. Finally, to complete our study, the hardware implementation complexity was discussed and it has been proved that the SDD detector is a good trade-off between performance and implementation complexity for deep space missions.

VIII. REFERENCES

[1] *CCSDS Recommendations For Space Data System Standards. Radio Frequency and Modulation Systems, Part 1, Earth Stations and Spacecraft*. CCSDS 401.0-B Blue Book, June 2001.

[2] M. K. Simon, *Bandwidth-efficient digital modulation with application to deep space communication*. Wiley & Sons, 2003.

[3] P. Laurent, "Exact and approximate construction of digital phase modulations by superposition of amplitude modulated pulses (AMP)," *IEEE Transaction on Communications*, vol. 34, no. 2, pp. 150-160, Feb 1986.

[4] E. Vassalo and M. Visintin "Carrier phase synchronization for GMSK signals", International Journal of Satellite Communication and Networking, pp. 391-415, 2002.

[5] S. Shambayati and D. K. Lee, "GMSK modulation for deep space applications," *Aerospace Conference, 2012 IEEE*, pp. 1-13, Big Sky, MT, 2012.

[6] John L. Stensby, *Phase-Locked LOOPS Theory and applications*. CRC Press, 1997.

[7] U. Mengali and A. N. D'Andrea, *Synchronization techniques for Digital Receivers*. PLENUM Press, 1997.

[8] Xu Li and Wang Qin, "CORDIC based algorithm for frequency offset estimation," *Communication Technology (ICCT), 2010 12th IEEE International Conference on, Nanjing*, pp. 817-820, 2010.

[9] A. Thomas "Combining Bandwidth and Power efficiency contribution of Third order PLL", *5th ESA International Workshop on Tracking, Telemetry and Command Systems for Space Applications*, Darmstadt, Germany, 2010.